0D–2D Quantum Dot: Metal Dichalcogenide Nanocomposite Photocatalyst Achieves Efficient Hydrogen Generation

Xiao-Yuan Liu, Hao Chen, Ruili Wang, Yuequn Shang, Qiong Zhang, Wei Li, Guozhen Zhang, Juan Su, Cao Thang Dinh, F. Pelayo García de Arquer, Jie Li, Jun Jiang, Qixi Mi, Rui Si, Xiaopeng Li, Yuhan Sun, Yi-Tao Long, He Tian, Edward H. Sargent, and Zhijun Ning**

Hydrogen generation via photocatalysis-driven water splitting provides a convenient approach to turn solar energy into chemical fuel. The development of photocatalysis system that can effectively harvest visible light for hydrogen generation is an essential task in order to utilize this technology. Herein, a kind of cadmium free Zn–Ag–In–S (ZAIS) colloidal quantum dots (CQDs) that shows remarkably photocatalytic efficiency in the visible region is developed. More importantly, a nanocomposite based on the combination of 0D ZAIS CQDs and 2D MoS_2 nanosheet is developed. This can leverage the strong light harvesting capability of CQDs and catalytic performance of MoS_2 simultaneously. As a result, an excellent external quantum efficiency of 40.8% at 400 nm is achieved for CQD-based hydrogen generation catalyst. This work presents a new platform for the development of high-efficiency photocatalyst based on 0D–2D nanocomposite.

Hydrogen provides an attractive means of storing renewable energy via large-scale energy buffering, as a chemical feedstock, and for transportation.[1,2] In photocatalysis, solar energy is used directly to synthesize chemical fuel directly.[1] Tremendous efforts have been made during the past decades to develop highly efficient photocatalysts for hydrogen generation, with impressive advances in metal oxides,[3–6] perovskites,[7–9] and metal dichalcogenides.[10,11] However, most light-harvesting materials suitable for photocatalysis rely on UV wavelength photoexcitation: for example, TiO_2, a material for photocatalytic applications and having a 3.2 eV bandgap, only harvests at most 4% of the solar spectrum as a result of its wide bandgap.[12,13] Materials with narrower bandgaps, such as CdS (2.78 eV, corresponding to ≈446 nm), have also been explored to extend the response into the visible.[14,15]

The development of nontoxic and efficient materials with visible-light response, including light with wavelengths well beyond CdS bandgap, represents one challenge on the path to higher efficiency photocatalysts. Metal sulfide materials such as $CuInS_2$[16] and $ZnS–AgInS_2$[17] have been widely explored as visible light harvesting materials for photocatalytic hydrogen generation. Their hydrogen evolution rates have generally lain

X.-Y. Liu, H. Chen, R. L. Wang, Y. Q. Shang, Dr. Q. Zhang, Dr. J. Su, Prof. Q. X. Mi, Prof. Z. J. Ning
School of Physical Science and Technology
ShanghaiTech University
Shanghai 201210, P. R. China
E-mail: ningzhj@shanghaitech.edu.cn

X.-Y. Liu, Prof. Y.-T. Long, Prof. H. Tian
Key Laboratory for Advanced Materials and Department of Chemistry
East China University of Science and Technology
Shanghai 200237, P. R. China
E-mail: ytlong@ecust.edu.cn

H. Chen, R. L. Wang, Y. Q. Shang
Shanghai Institute of Ceramic
Chinese Academy of Science
Shanghai 200050, P. R. China

H. Chen, R. L. Wang, Y. Q. Shang
School of Chemistry and Chemical Engineering
University of Chinese Academy of Science
Beijing 100049, P. R. China

DOI: 10.1002/adma.201605646

Dr. W. Li, Dr. R. Si
Shanghai Institute of Applied Physics
Chinese Academy Science
Shanghai Synchrotron Radiation Facility
Shanghai 201204, P. R. China

Dr. G. Z. Zhang, Prof. J. Jiang
School of Chemistry and Materials Science
Hefei National Laboratory for Physical Sciences at the Microscale
and CAS Key Laboratory of Mechanical Behavior and
Design of Materials (LMBD)
University of Science and Technology of China (USTC)
Hefei 230026, P. R. China

Dr. C. T. Dinh, Dr. F. P. G. de Arquer, Dr. J. Li, Prof. E. H. Sargent
Department of Electrical and Computer Engineering
University of Toronto
10 King's College Road, Toronto, Ontario M5S 3G4, Canada

Prof. X. Li, Prof. Y. Sun
CAS Key Laboratory of Low-Carbon Conversion Science and Engineering
Shanghai Advanced Research Institute (SARI)
Chinese Academy of Sciences (CAS)
Shanghai 201210, P. R. China

below 10 mmol h^{-1} g^{-1} under AM1.5G simulated light illumination. This low reaction rate is due to poor carrier transfer from the light harvesting center to catalysts, as well as to the presence of deep energy level defects that act as recombination centers (Table S1, Supporting Information).

Quantum-confined materials, such as quantum dots (QDs), have recently shown promise for efficient photocatalysis.[18–21] Compared with bulk materials, QDs benefit from bandgap tunability, strong light harvesting capability in the visible and near-infrared region, and large surface to volume ratio.[22–26] In recent years, QDs have been reported as efficient light harvesting materials for hydrogen generation.[24–29] Great progress has been made for cadmium-based QDs via optimization of the synthesis procedure and ligands, as well as cocatalysts (Table S2, Supporting Information).[30,31] Meanwhile, the use of appropriate organic sacrificial reagents facilitates holes harvesting from QDs and brings higher hydrogen generation efficiency. Some organic sacrificial reagents, such as ascorbic acid (AA), possess sustainability character, and the value of the oxidation products could be improved in comparison to the original reagent.[32] Recently, a stable quantum efficiency (the number H_2 molecules that evolve per incident photon) of 36% at 520 nm has been achieved based on colloidal CdSe QDs using AA as the sacrificial reagent.[33] This is in contrast to cadmium-free QDs systems, which have been reported to yield much lower efficiencies. It is believed that deep energy level defects in the bandgap, as well as poor carrier separation in these materials, may be responsible for the lower performance of previously reported Cd-free materials.

Here we address directly the important challenge of creating Cd-free materials for high-efficiency photocatalysts using a novel approach. We introduce glutathione (GSH) surface ligands to implement a new cadmium-free Zn–Ag–In–S (ZAIS) QDs synthesis.[34] Our approach results in highly stable and low-defect QDs with significantly enhanced efficiency of photocatalytic hydrogen generation compared with all prior Cd-free materials. We combine these materials with 2D MoS_2 via self-assembly process to create photocatalyst nanocomposites. The large surface area of 2D MoS_2 allows the robust anchoring of QDs onto its surface. This facilitates efficient electron injection from QDs to 2D MoS_2. Our ZAIS–MoS_2 nanocomposites exhibit excellent catalytic capabilities for hydrogen generation with a quantum efficiency of 41% at 400 nm (Table S2, Supporting Information).

We utilized $Zn(Ac)_2$, $AgNO_3$, $In(Ac)_3$ as cation precursors, Na_2S as anion precursor, and GSH as ligands for ZAIS QDs synthesis.[34] Water was utilized as the growing solvent to avoid ligand exchange for QDs synthesized in an oil solvent. GSH ligands that comprise thiol, carboxy and amino groups make ZAIS QDs highly stable in water under various pH values. In order to obtain the optimal bandgap structure, we carefully modulated the composition and the ratio of cations in ZAIS QDs (**Figure 1**; Figures S1–S7 and Tables S3 and S4, Supporting Information). ZAIS QDs with increasing Ag amount are denoted as ZAIS-1, ZAIS-2, ZAIS-3, and ZAIS-4. With increasing Ag content, a red shift is detected both in the absorption and fluorescence spectra, indicative of a bandgap decrease (Figure 1a,b). ZAIS-2 QDs show the highest photoluminescence quantum yield (PLQY) of 31.4%, where the ratio of Ag and In is 1 to 10. This is indicative of a significantly lower density of deep energy level defects. Ternary nanomaterials Zn–Ag–S (ZAS), Ag–In–S (AIS), and Zn–In–S (ZIS) were synthesized for comparison (Figures S2–S7, and Table S3, Supporting Information). All of them exhibit either narrow bandgap or short adsorption wavelength range with a low PLQY, showcasing the crucial beneficial effect of incorporating Ag in ZAIS materials.

We employed X-ray diffraction (XRD) analysis to reveal the crystal structure of ZAIS QDs. All ZAIS QDs show a zincblende

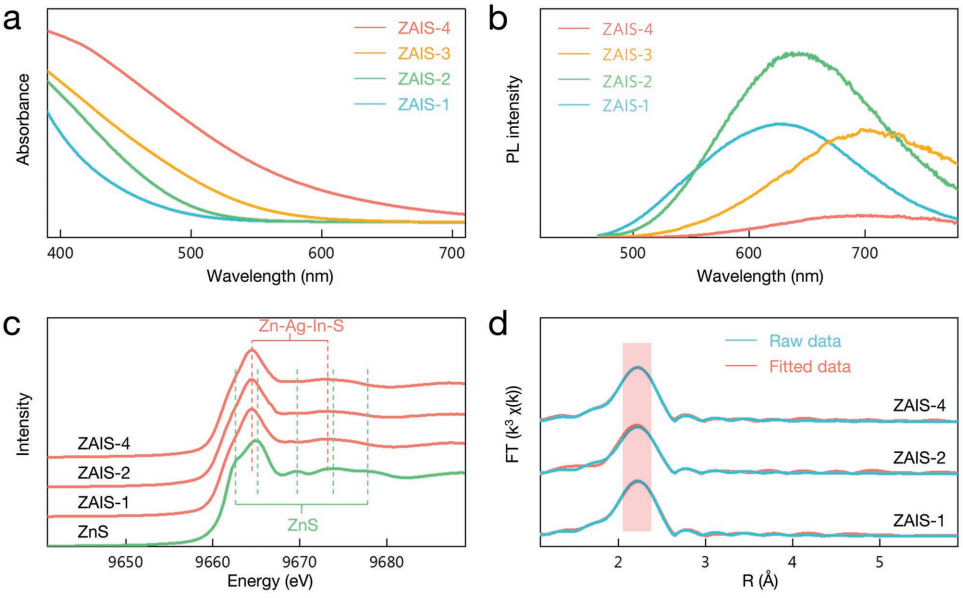

Figure 1. a) Absorption spectra of ZAIS QDs. As the increase of Ag content, the absorption spectra range is red-shifted. b) Photoluminescence spectra of ZAIS QDs. c) Zn K-edge XANES profiles for ZAIS QDs. No obvious change can be observed with different amount of Ag. d) Zn K-edge EXAFS spectra in *R* space for ZAIS QDs with different amount of Ag. All samples show similar R space value.

crystal structure, with no obvious changes as changing the amount of Ag (Figure S1, Supporting Information). The X-ray absorption near-edge spectroscopy (XANES) and extended X-ray absorption fine structure (EXAFS) were employed to study the electronic and local structures of the ZAIS QDs. Zn K-edge XANES profiles indicate that all the Zn species in ZAIS QDs are Zn^{2+}, similar to that of ZnS (Figure 1c). EXAFS measurements (Figure 1d) demonstrate that all ZAIS QDs exhibit a prominent peak at 2.3–2.4 Å assigned to the Zn−S bond with a coordination number (CN) of ≈4 (Table S5, Supporting Information), which is consistent with the zincblende QD structure. No other characteristic peaks, such as Zn–Zn contribution at longer distances (>2.5 Å), were observed, revealing the pure Zn–S interaction in ZAIS QDs.

We then prepared 2D MoS_2 nanosheets by delaminating MoS_2 bulk material using ultrasonication.[35,36] 0D–2D QDs–MoS_2 nanocomposites were fabricated by ultrasonically mixing ZAIS-2 QDs and MoS_2 nanosheets in aqueous solution. Anchoring of QDs to 2D materials' surface can occur by static charge attraction between QDs ligand anions and the sulfur vacancies on MoS_2 nanosheet (**Figure 2**f).[37] We analyzed the morphology of the as-produced ZAIS-2 QDs–MoS_2 nanocomposites using transmission electron microscopy (TEM) (Figure 2). ZAIS-2 QDs (3–5 nm) are uniformly distributed on the surface of MoS_2 nanosheet (Figure 2a,b). High-resolution TEM (HRTEM) images of ZAIS-2 QD show a lattice fringe with a spacing of 0.23 nm (Figure 2c,e), corresponding to the (111) facet. The HRTEM image of 2D MoS_2 nanosheet displays the expected hexagonal MoS_2 nanostructure with a lattice spacing of 0.28 nm, belonging to (100) facet of MoS_2 (Figure 2d).[38] Atomic force microscopy (AFM) measurements demonstrate that the thickness of the as-prepared 2D MoS_2 nanosheet is ≈3–4 nm, corresponding to 5–8 MoS_2 layers (Figure S8, Supporting Information), confirming its 2D structure.[36]

We studied the band structure of ZAIS-2 and MoS_2 nanosheets via photophysical and electrochemical methods. ZAIS-2 QDs exhibit an absorbance edge at 560 nm and a photoluminescence (PL) peak at 644 nm (**Figure 3**a). Using a Tauc plot, we estimated the energy bandgap (E_g) of ZAIS-2 QDs to be 2.20 eV, which is smaller than that of CdS (Figure 3b). The conduction band (CB) energy level is measured by electrochemical Mott–Schottky analysis. QDs show an n-type semiconductors character with flat band position of –0.91 V versus normal hydrogen electrode (NHE) at pH 7.0 (Figure 3c). Considering the high doping density of the samples calculated from the Mott–Schottky curves,[39] we assume that the position of the conduction band is the same as that of the flat band.[40,41] The valence band (VB) position is 1.29 V against NHE calculated based on E_g and CB level. The MoS_2 nanosheets show a characteristic peak at 672 nm.[35] The flat band position of MoS_2 nanosheets is –0.73 V versus NHE based on Mott–Schottky analysis. Under different frequencies, no notable difference of the band positions was obtained for both ZAIS-2 QDs and MoS_2 nanosheets (Figure S9, Supporting Information). The diagram for the band structure of the nanocomposite indicates that the CB position of ZAIS-2 QDs is shallower than that of MoS_2, which facilitates electron migration from ZAIS-2 QDs to MoS_2 (Figure 3d).

We then investigated the photocatalytic hydrogen generation performance of ZAIS-2 QDs. ZAIS-2 QDs were firstly dispersed in water with AA as a sacrificial reagent and then Ni complex was used as the cocatalyst under visible light illumination (400–780 nm, 95 mW cm^{-2}). Photocatalytic conditions, such as pH value, QDs and AA concentration, play important roles in the photocatalytic performance (Figure S10, Supporting Information). The highest catalytic activity was achieved when 0.1 mg mL^{-1} photocatalyst, 0.2 M AA, water at pH 5.0 were used in the reaction system. **Figure 4** shows the hydrogen production rate of different samples under the optimized

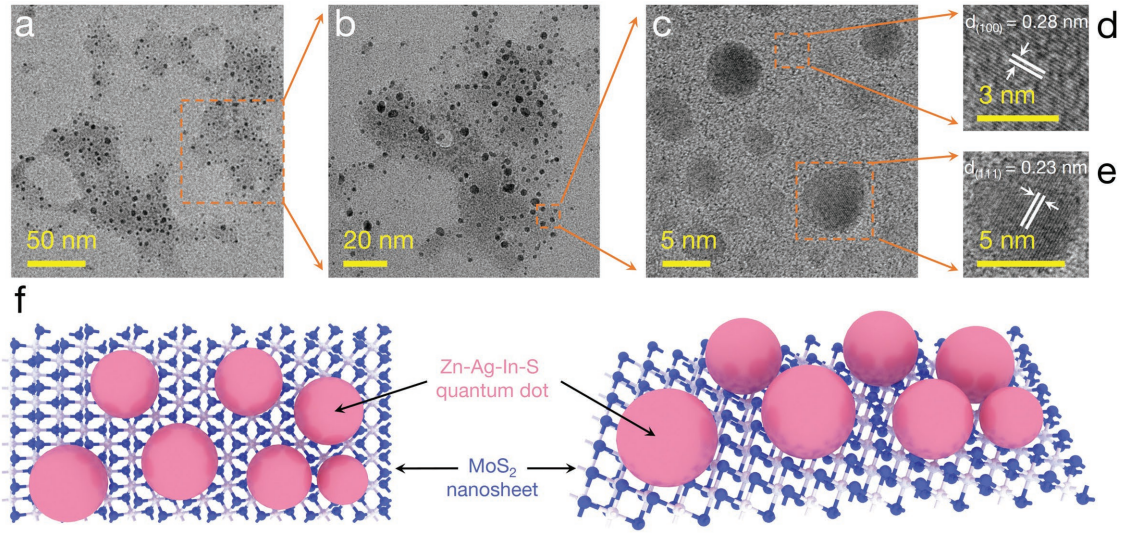

Figure 2. Structures of ZAIS-2 QDs–2D MoS_2 nanocomposites. a,b) TEM images of ZAIS-2 QDs–MoS_2 nanocomposites. Almost all QDs are homogeneously dispersed on MoS_2 nanosheet. c) A magnified TEM image of ZAIS-2 QDs located on single MoS_2 nanosheet. d) HRTEM images of MoS_2 nanosheet. The lattice fringes of 0.28 nm are indexed to the (100) planes. e) HRTEM image of ZAIS-2 QDs anchored on MoS_2 nanosheet. The lattice fringes of 0.23 nm are indexed to the (111) planes. f) Schematic of ZAIS-2 QDs–2D MoS_2 nanocomposite.

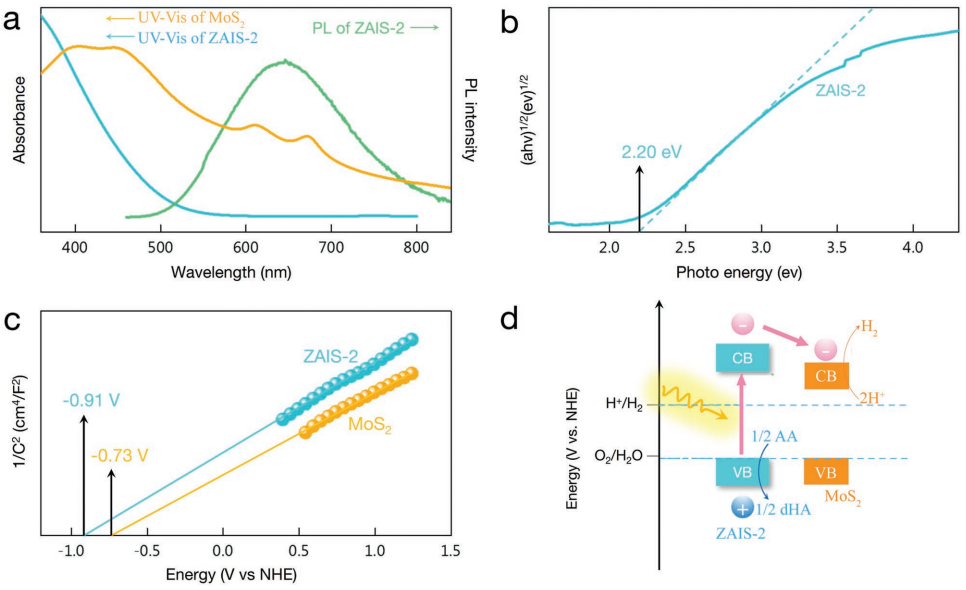

Figure 3. Optical properties and band structures of ZAIS-2 QDs and MoS_2 nanosheet. a) Absorption spectra of ZAIS-2 QDs and MoS_2 nanosheet, and photoluminescence spectrum of ZAIS-2 QDs. b) $(\alpha h\nu)^{1/2}$ versus $h\nu$ curve of ZAIS-2 QDs. The bandgap is determined to be 2.2 eV. c) Mott–Schottky plots of ZAIS-2 QDs and MoS_2 nanosheet. The conduction band position of QDs is higher than that of MoS_2, allowing efficient electron injection from QDs to MoS_2. d) Band structures for the hydrogen generation system and electron–hole transfer processes in ZAIS-2 QDs–MoS_2 nanocomposite. Electrons generated in QDs can transfer from the conduction band of QDs to MoS_2, while the holes are reduced by the sacrificial reagent.

conditions. ZAIS-2 QDs display a hydrogen generation rate of 21.0 mmol h^{-1} g^{-1} (the rate was measured after 3 h of continuous irradiation) when using Ni-dihydrolipoic acid (Ni-DHLA) as cocatalyst.[42] In the absence of the cocatalyst, ZAIS-2 QDs show a H_2 evolution rate of 16.3 mmol h^{-1} g^{-1}. These results demonstrate that ZAIS QDs are efficient photocatalysts for hydrogen generation even without cocatalyst. No hydrogen is detected in the absence of light or ZAIS-2 QDs, indicating that

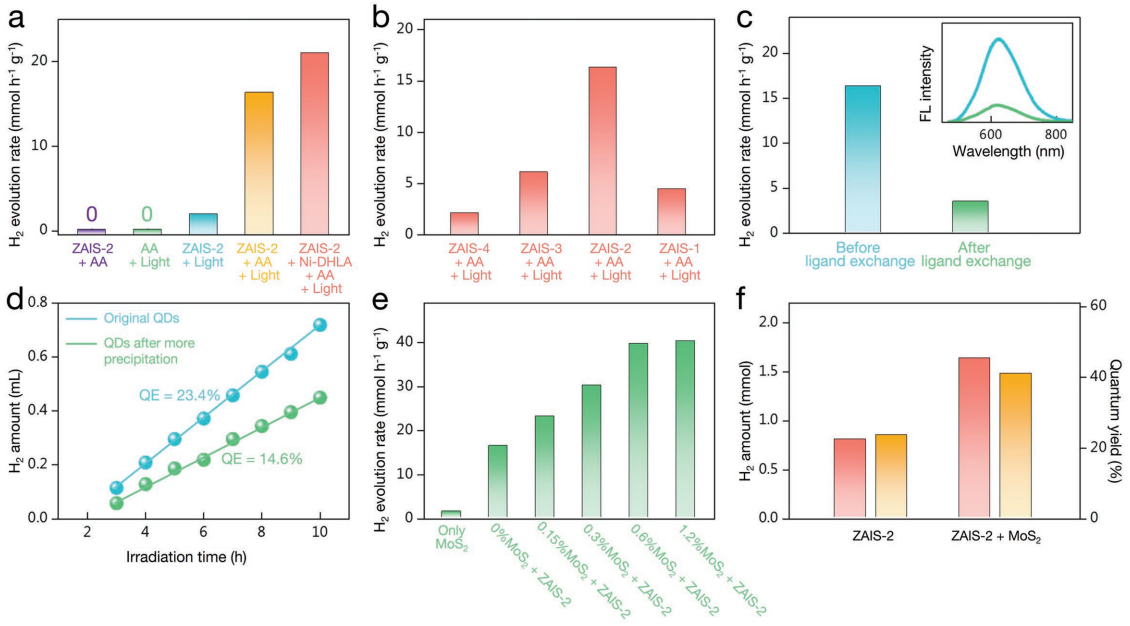

Figure 4. Hydrogen generation performances of ZAIS QDs and ZAIS-2 QDs–MoS_2 nanocomposites. a) Photocatalytic hydrogen generation of ZAIS-2 QDs under different conditions with visible light irradiation. b) Photocatalytic hydrogen generation of ZAIS QDs with different ratio of Ag and In. c) Hydrogen generation and fluorescent spectra of ZAIS-2 QDs before and after ligand exchange using DHLA. d) Photocatalytic hydrogen generation and quantum efficiencies of ZAIS-2 QDs under different washing conditions at 400 nm with 25% attenuation slice. e) Photocatalytic hydrogen generation of ZAIS-2 QDs with different amounts of MoS_2nanosheet. f) Hydrogen generation amount in 5 h irradiation and quantum efficiency of ZAIS-2 QDs and QDs–MoS_2nanocomposite at 400 nm with a 25% attenuation slice. As the addition of MoS_2, the hydrogen generated is much increased, as well as the quantum efficiency.

hydrogen generation indeed derives from photocatalysis via QDs. Only a trace of hydrogen is generated in the AIS and ZAS nanomaterial-based systems (Figure S11, Supporting Information), which could be ascribed to either a deep CB position or bandgap defects (Figure S2, Supporting Information). The poor performance of ZIS QDs is ascribed to the absence of silver whose crucial role in high-quality photophysical properties was documented above.

To clarify the mechanism behind hydrogen generation and distinguish hydrogen generation from water and AA, we replaced H_2O for D_2O as the solvent. We analyzed the generated gas products by gas chromatography–mass spectrometer (GC–MS). H_2, DH, and D_2 were detected (Figure S12, Supporting Information). The amount of D_2 is much higher than H_2 and DH, indicating that D_2O is the main proton source. To further confirm that hydrogen generation stems from water splitting, we performed photocatalysis in pure water without the sacrificial agent. Even in the absence of AA, hydrogen generation rate of 1.94 mmol h^{-1} g^{-1} is obtained. When AA was used as the sacrificial agent, the amount of generated hydrogen increases by 8.4 times due to efficient extraction of photoholes generated from QDs. We carried out time-dependent ^{13}C NMR analysis to track down the oxidation of AA. As the reaction evolves, bicyclic dehydroascorbic acid hydrate and dehydroascorbic acid dehydrate were detected in sequence (Figure S13, Supporting Information).[33] This indicates that AA reacts firstly with holes from the QDs to generate dehydroascorbic acid and two protons. In water dehydroascorbic acid predominantly exists as the dehydroascorbic acid hydrate, which subsequently reacts with water to produce dehydroascorbic acid dehydrate.[43] The photocatalytic solution contains D^+ and H^+, thus D_2, H_2, and DH were detected by GC–MS. The amount of photocatalytic generated D_2 is much higher than H_2 and DH owing to the fact that the concentration of generated H^+ from the oxidation of AA is much lower than that of D^+ in D_2O.

We compared the performances of four kinds of ZAIS QDs with varying Ag content. ZAIS-2 QD shows the highest hydrogen generation rate, which we attributed to its optimized bandgap and low defect concentration (Figure 4b). We measured the quantum efficiency at the single wavelength to study the ratio of carriers utilized for hydrogen generation.[33,44] At 400 nm, ZAIS-2 QDs show a quantum efficiency of 23.4%, comparable to the highest value reported for cadmium-based QDs, and higher than reported cadmium-free QDs (Tables S1 and S2, Supporting Information). Efficient hydrogen generation is still observed when the illumination wavelength is extended over 500 nm (Figure S14, Supporting Information).

In order to ascertain the role of surface passivation in achieving efficient hydrogen evolution, we employed a ligand exchange process to DHLA–QDs for comparison. The PL intensity of QDs after ligand exchange with DHLA is dramatically reduced compared with GSH, indicating the increase of defects on QDs surface (Figure 4c). The photocatalytic performance decreased dramatically from 16.3 to 3.45 mmol h^{-1} g^{-1}. Deep energy level defects can result in a fast carriers recombination channel before carrier separation.[45] On the other hand, considering the narrow bandgap of visible active semiconductor materials, the energy level of the defects may be located below the hydrogen reduction position, and in this way, trapped electrons will be unable of driving hydrogen generation.

We further compared the hydrogen generation performance of QDs with different solvent precipitation times. It is well accepted that the nonsolvent precipitation process could induce ligand loss and the formation of defects.[46] When we increased precipitation times by employing ethanol as nonsolvent, the photocatalytic activities of ZAIS-2 QDs decreased from 23% to 15%, demonstrating the deleterious effect of defects in the catalytic performance (Figure 4d), although QDs are dispersed well in water after the modification. Considering the large surface to volume ratio of QDs, we anticipate that efficient surface passivation is, therefore, critical to realize high photocatalytic performance.

In order to improve carrier separation efficiency, we explored the ZAIS-2 QDs–MoS_2 nanocomposite for hydrogen generation. First, we investigated the static and transient photophysical behavior of the nanocomposite. After the addition of MoS_2 nanosheets, both PL intensity and PL lifetime of QDs are reduced (**Figure 5**a,b), indicating efficient carriers migration from QDs to nanosheet. The anchoring of QDs on MoS_2 enables direct contact between QDs and MoS_2, facilitating carrier transport from QDs to MoS_2. Due to the shallower CB energy level of ZAIS-2 QDs, electrons are injected from QDs into the nanosheets. At the same time, the VB level of QDs is below than that of AA, allowing holes transfer from QDs to AA. We further measured the static and transient photophysical behavior of QDs under the addition of AA (Figure 5c,d). The addition of AA to QDs results in a significant reduction of both PL intensity and PL lifetime, indicating that efficient hole transfers from QDs to AA. Even in the presence of MoS_2, the addition of AA further reduces PL intensity and lifetime, confirming again the efficient holes transfer from QDs to AA.

We subsequently measured the hydrogen generation performance of the nanocomposite. After the addition of MoS_2, the hydrogen generation efficiency is significantly increased (Figure 4e). When the amount of MoS_2 nanosheet is 0.60 wt%, a peak quantum efficiency of 41% under 400 nm light illumination is realized. Further increasing MoS_2 amount did not lead to distinctly higher efficiency, possibly due to the light scattering of 2D nanosheet. As shown in Figure 4f, 1.63 mmol (36.52 mL at standard temperature and pressure) of hydrogen is produced for nanocomposite with 0.60 wt% MoS_2 in 5 h. This is two times higher than that of bare QDs counterparts. ZAIS-2 QDs show stable hydrogen generation, and no obvious change of the absorbance spectra is observed after 10 h of reaction (Figure 4d; Figure S15, Supporting Information), which is comparable to Cd-QD-based photocatalytic system.

In conclusion, we report the first high-efficiency cadmium-free QD photocatalysts for hydrogen generation. We reduce dramatically the presence of deep energy level defects in Cd-free materials by synthesizing ZAIS QDs that are optimized via compositional engineering. This leads to a hydrogen generation quantum efficiency of 23.4% at 400 nm. Nanocomposites based on 0D ZAIS-2 QDs and 2D MoS_2 were also developed for photocatalytic hydrogen generation, leading to a quantum efficiency of 41% at 400 nm (hydrogen generation rate of 40.1 mmol h^{-1} g^{-1} under standard visible light illumination). Efficient carrier transport between QDs and MoS_2 is

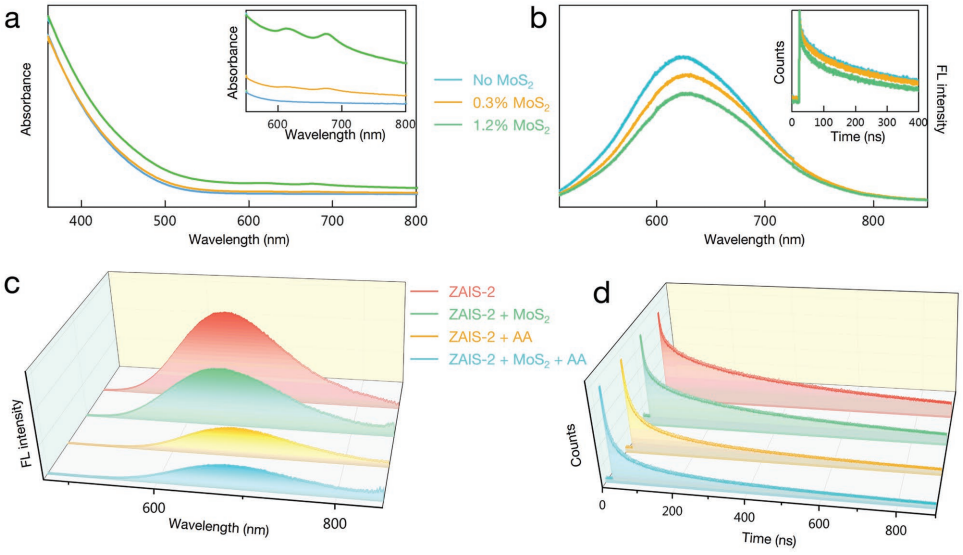

Figure 5. Carriers migration in ZAIS-2 QDs–MoS_2nanosheet-based nanocomposites. a) UV–vis absorption spectra of nanocomposite with different amounts of MoS_2nanosheet; inset in Figure a shows the amplified UV–vis absorption spectra of the nanocomposite from 560 to 800 nm. b) Photoluminescence spectra of nanocomposites with different amounts of MoS_2 nanosheet; inset in Figure b shows fluorescence lifetime spectra of QDs in nanocomposites as the change of MoS_2 concentration. As the increase of MoS_2 concentration, both PL intensity and PL lifetime are decreased. c) Photoluminescence spectra and d) fluorescence lifetime of ZAIS-2 QDs, ZAIS-2 QDs with AA, ZAIS-2-0.6% MoS_2 nanocomposite and the nanocomposite with AA. Significant reduction of PL intensity and lifetime were observed as the addition of AA, indicating efficient holes transfer from QDs to AA.

confirmed by photoluminescence studies. Given the reduction capability and affinity on QDs surface of the sacrificial reagents are important for holes harvesting, screening of sacrificial molecules can be employed to improve hydrogen generation efficiency further. The combination of QDs and 2D nanosheet combines the strong light harvesting capability of QDs with the excellent catalytic performance of 2D nanosheets. This work presents a platform for the construction of high-efficiency photocatalytic systems for hydrogen generation that could potentially be extended toward carbon dioxide reduction and oxygen evolution.

Experimental Section

Synthesis of ZAIS QDs: 2.0 mmol $Zn(Ac)_2$, 4.0 mmol $In(Ac)_3$, 40.0 mmol GSH and different amount of $AgNO_3$ (0.2, 0.4, 0.8, and 2.0 mmol, and the synthesized ZAIS QDs were denoted as ZAIS-1 QDs, ZAIS-2 QDs, ZAIS-3 QDs, and ZAIS-4 QDs, respectively) were dissolved in 250 mL water and the pH was adjusted to 8.5 using NaOH solution. After injected 10 mL 2.6 mmol $Na_2S{\cdot}9H_2O$ solution, the mixture was refluxed 4.5 h under 100 °C in the open-air atmosphere; then ZAIS QDs were precipitated by the addition of ethanol and dried at 40 °C under vacuum.[34] ZAS, AIS, and ZIS nanomaterials were synthesized using the same method as ZAISQDs.

Preparation of MoS_2 Nanosheets and ZAIS–MoS_2 Nanocomposite: 30 mg bulk MoS_2 (<2 × 10^{-6} M) was dispersed in 4.5 mL ethanol and 5.5 mL water, then the mixture was ultrasonicated for 8 h. After centrifuged at 3000 rpm for 10 min, the supernatant was collected for the photocatalysis.[35,36] 10 mg ZAIS QDs and different amount of MoS_2 nanosheet were dissolved in 10 mL water and ultrasonicated for 2 h to obtain the ZAIS QDs–MoS_2 nanocomposite.

Characterization: UV–vis absorption spectra were recorded on a Cary Series UV-Vis-NIR Spectrophotometer. Fluorescent spectra were recorded using HORIBA FL-3000/RM4-3000 spectrophotometer. ^{13}C NMR spectra were acquired in D_2O on BRUKER AVANCE 500 spectrometer. X-ray photoelectron spectroscopy was obtained using ESCALAB 250Xi X-ray photoelectron spectrometer (Thermo Fisher) with Al Kα X-ray source. XRD patterns were recorded using Bruker D2 PHASER X-ray diffractometer. TEM images were taken on a JEM 2100 at an accelerating voltage of 200 kV. AFM images were measured on MFP-3D-BIO using tapping-mode.

X-ray Fine Structure (XAFS) Measurements: XAFS spectra at Zn K-edge (E_0 = 9659 eV) were performed at BL14W1 beamline of Shanghai Synchrotron Radiation Facility operated at 3.5 GeV under "top-up" mode with a constant current of 220 mA. The XAFS data on ZAIS QDs were recorded under transmission mode with ion chambers. The energy was calibrated accordingly to the absorption edge of pure Zn foil. Athena and Artemis codes were used to extract the data and fit the profiles. For theXANES part, the experimental absorption coefficients as a function of energies $\mu(E)$ were processed by background subtraction and normalization procedures, which were reported as "normalized absorption." For the EXAFS part, the Fourier transformed data in R space were analyzed by applying the first shell approximation model for the ZnS shell. The passive electron factors, S_0^2, were determined by fitting the experimental Zn foil data and fixing the Zn–Zn coordination number (CN) to be 12, and then fixed for further analysis of the measured samples. The parameters describing the electronic properties (e.g., correction to the photoelectron energy origin, E_0) and local structure environment including CN, bond distance (R), and Debye Waller (D.W.) factor around the absorbed atoms were allowed to vary during the fit process.

Electrochemical Measurements: The Mott–Schottky experiments were conducted on an electrochemical workstation (CHI660E, Shanghai Chenhua Limited, China) and a three-electrode system. The materials modified fluoride-doped tin oxide (FTO), a saturated calomel electrode (SCE), and a platinum wire were used as working, reference and counter electrodes, respectively; 0.5 M Na_2SO_4 aqueous solution (pH7.0) was used as electrolyte. 2 mg ZAIS QDs or ZAIS QDs-0.6%MoS_2 were dispersed in 2 mL water and 1 mL 5% Nafion solution; then 10 µL mixture was dropped on FTO and dried using an IR lamp. Mott–Schottky plots were evaluated at the potential range of 1–−1 V versus SCE at a frequency of 1 kHz.

Photocatalysis of Hydrogen Generation: A 100 mL solution containing 10 mg ZAIS QDs or ZAIS QDs–MoS_2 nanocomposite and AA at different

pH values were prepared and dropped to a 250 mL reactor. The reactor was placed into a temperature-controlled block at 25 °C and degassed to remove the air and irradiated from the top of the reactor using a 300 W Xe-lamp with 15 A working current. A cutoff filter was used to obtain the visible light (>400 nm) and generated hydrogen was analyzed using online gas chromatography with TCD detector and a 5 Å molecular sieve column.

Quantum Efficiency Measurements: The quantum efficiencies of ZAIS QDs and ZAIS QDs–MoS_2 nanocomposite at single wavelength were calculated using the same methods according to the reported works.[33,44] Generally, the intensities of the single wavelength light that passes through the sample and blank solution were measured using a CEL-NP2000 power meter. The different of light intensities between the sample and blank solution was considered to be the absorbed by the ZAIS QDs and ZAIS QDs–MoS_2. The quantum efficiency was calculated using the following formulas

$$P = \frac{c \times h \times n}{\lambda \times t} \quad (1)$$

$$q_p = n/t \quad (2)$$

$$\phi = 2k/q_p \quad (3)$$

where P is the light intensity (Watts), k is the hydrogen generation rate (mol s^{-1}), ϕ is the quantum efficiency, λ is the single wavelength, h is the Planck's constant (J s^{-1}), c is the light speed (m s^{-1}), n is the photons number, t is the irradiation time (s), and q_p is the photo flux (number s^{-1}).

Supporting Information

Supporting Information is available from the Wiley Online Library or from the author.

Acknowledgements

X.-Y.L. and H.C. contributed equally to this work. This work was supported by the start-up funding from ShanghaiTech University, the Young 1000 Talents Program, National Science Fund of China (U1632118, 21571129, 21373259), National Basic Research 973 Program (2016YFA0204000 and 2013CB733700), Shanghai Key Research Program (16JC1402100), Shanghai International Cooperation Project (16520720700), Science Fund for Creative Research Groups (21421004), Strategic Priority Research Program of the CAS (XDA09030102), and the Hundred Talents project of the Chinese Academy of Sciences. The authors highly thank the Test Center of ShangHaiTech University, National Center for Protein Science (Shanghai) and Shanghai Light Source for Synchrotron Radiation measurement assistance.

Conflict of Interest

The authors declare no conflict of interest.

Keywords

0D–2D nanocomposites, hydrogen generation, MoS_2 nanosheets, photocatalysis, quantum dots

Received: October 19, 2016
Revised: February 26, 2017
Published online: April 11, 2017

[1] N. Armaroli, V. Balzani, *ChemSusChem* **2011**, *4*, 21.
[2] B. A. Pinaud, J. D. Benck, L. C. Seitz, A. J. Forman, Z. Chen, T. G. Deutsch, B. D. James, K. N. Baum, G. N. Baum, S. Ardo, H. Wang, E. Miller, T. F. Jaramillo, *Energy Environ. Sci.* **2013**, *6*, 1983.
[3] A. A. Tahir, K. G. U. Wijayantha, S. Saremi-Yarahmadi, M. Mazhar, V. McKee, *Chem. Mater.* **2009**, *21*, 3763.
[4] K. E. DeKrafft, C. Wang, W. Lin, *Adv. Mater.* **2012**, *24*, 2014.
[5] G. Carraro, C. Maccato, A. Gasparotto, T. Montini, S. Turner, O. I. Lebedev, V. Gombac, G. Adami, G. Van Tendeloo, D. Barreca, P. Fornasiero, *Adv. Funct. Mater.* **2014**, *24*, 372.
[6] R. Li, Y. Weng, X. Zhou, X. Wang, Y. Mi, R. Chong, H. Han, C. Li, *Energy Environ. Sci.* **2015**, *8*, 2377.
[7] J. Luo, J.-H. Im, M. T. Mayer, M. Schreier, M. K. Nazeeruddin, N.-G. Park, S. D. Tilley, H. J. Fan, M. Grätzel, *Science* **2014**, *345*, 1593.
[8] J. Luo, Z. Li, S. Nishiwaki, M. Schreier, M. T. Mayer, P. Cendula, Y. H. Lee, K. Fu, A. Cao, M. K. Nazeeruddin, Y. E. Romanyuk, S. Buecheler, S. D. Tilley, L. H. Wong, A. N. Tiwari, M. Grätzel, *Adv. Energy Mater.* **2015**, *5*, 1501520.
[9] Gurudayal, D. Sabba, M. H. Kumar, L. H. Wong, J. Barber, M. Gratzel, N. Mathews, *Nano Lett.* **2015**, *15*, 3833.
[10] Q. Xiang, J. Yu, M. Jaroniec, *J. Am. Chem. Soc.* **2012**, *134*, 6575.
[11] Q. Lu, Y. Yu, Q. Ma, B. Chen, H. Zhang, *Adv. Mater.* **2016**, *28*, 1917.
[12] J. Schneider, M. Matsuoka, M. Takeuchi, J. Zhang, Y. Horiuchi, M. Anpo, D. W. Bahnemann, *Chem. Rev.* **2014**, *114*, 9919.
[13] S. G. Kumar, L. G. Devi, *J. Phys. Chem. A* **2011**, *115*, 13211.
[14] K. A. Brown, M. B. Wilker, M. Boehm, G. Dukovic, P. W. King, *J. Am. Chem. Soc.* **2012**, *134*, 5627.
[15] T. Simon, N. Bouchonville, M. J. Berr, A. Vaneski, A. Adrovic, D. Volbers, R. Wyrwich, M. Doblinger, A. S. Susha, A. L. Rogach, F. Jackel, J. K. Stolarczyk, J. Feldmann, *Nat. Mater.* **2014**, *13*, 1013.
[16] Y.-J. Yuan, D.-Q. Chen, Y.-W. Huang, Z.-T. Yu, J.-S. Zhong, T.-T. Chen, W.-G. Tu, Z.-J. Guan, D.-P. Cao, Z.-G. Zou, *ChemSusChem* **2016**, *9*, 1003.
[17] M. Jagadeeswararao, S. Dey, A. Nag, C. N. R. Rao, *J. Mater. Chem. A* **2015**, *3*, 8276.
[18] F. W. Wise, *Acc. Chem. Res.* **2000**, *33*, 773.
[19] J. Zhao, M. A. Holmes, F. E. Osterloh, *ACS Nano* **2013**, *7*, 4316.
[20] M. A. Holmes, T. K. Townsend, F. E. Osterloh, *Chem. Commun.* **2012**, *48*, 371.
[21] S. K. Apte, S. N. Garaje, S. D. Naik, R. P. Waichal, J. O. Baeg, B. B. Kale, *Nanoscale* **2014**, *6*, 908.
[22] A. J. Nozik, M. C. Beard, J. M. Luther, M. Law, R. J. Ellingson, J. C. Johnson, *Chem. Rev.* **2010**, *110*, 6873.
[23] K. A. Brown, S. Dayal, X. Ai, G. Rumbles, P. W. King, *J. Am. Chem. Soc.* **2010**, *132*, 9672.
[24] A. Das, Z. Han, G. M. Haghighi, R. Eisenberg, *Proc. Natl. Acad. Sci.* **2013**, *110*, 16716.
[25] B. C. Martindale, G. A. Hutton, C. A. Caputo, E. Reisner, *J. Am. Chem. Soc.* **2015**, *137*, 6018.
[26] J. Liu, Y. Liu, N. Liu, Y. Han, X. Zhang, H. Huang, Y. Lifshitz, S.-T. Lee, J. Zhong, Z. Kang, *Science* **2015**, *347*, 970.
[27] F. Wang, W. J. Liang, J. X. Jian, C. B. Li, B. Chen, C. H. Tung, L. Z. Wu, *Angew. Chem., Int. Ed.* **2013**, *52*, 8134.
[28] J. X. Jian, Q. Liu, Z. J. Li, F. Wang, X. B. Li, C. B. Li, B. Liu, Q. Y. Meng, B. Chen, K. Feng, C. H. Tung, L. Z. Wu, *Nat. Commun.* **2013**, *4*, 2695.
[29] F. Wang, W. G. Wang, X. J. Wang, H. Y. Wang, C. H. Tung, L. Z. Wu, *Angew. Chem., Int. Ed.* **2011**, *50*, 3193.
[30] P. Wang, J. Zhang, H. He, X. Xu, Y. Jin, *Nanoscale* **2015**, *7*, 5767.
[31] C. M. Chang, K. L. Orchard, B. C. M. Martindale, E. Reisner, *J. Mater. Chem. A* **2016**, *4*, 2856.
[32] M. Cargnello, A. Gasparotto, V. Gombac, T. Montini, D. Barreca, P. Fornasiero, *Eur. J. Inorg. Chem.* **2011**, *2011*, 4309.

[33] Z. Han, F. Qiu, R. Eisenberg, P. L. Holland, T. D. Krauss, *Science* **2012**, *338*, 1321.
[34] D. Deng, J. Cao, L. Qu, S. Achilefu, Y. Gu, *Phys. Chem. Chem. Phys.* **2013**, *15*, 5078.
[35] J. N. Coleman, M. Lotya, A. O'Neill, S. D. Bergin, P. J. King, U. Khan, K. Young, A. Gaucher, S. De, R. J. Smith, I. V. Shvets, S. K. Arora, G. Stanton, H.-Y. Kim, K. Lee, G. T. Kim, G. S. Duesberg, T. Hallam, J. J. Boland, J. J. Wang, J. F. Donegan, J. C. Grunlan, G. Moriarty, A. Shmeliov, R. J. Nicholls, J. M. Perkins, E. M. Grieveson, K. Theuwissen, D. W. McComb, P. D. Nellist, V. Nicolosi, *Science* **2011**, *331*, 568.
[36] K. G. Zhou, N. N. Mao, H. X. Wang, Y. Peng, H. L. Zhang, *Angew. Chem., Int. Ed.* **2011**, *50*, 10839.
[37] Y. Lu, D. Wang, P. Yang, Y. Du, C. Lu, *Catal. Sci. Technol.* **2014**, *4*, 2650.
[38] X. Huang, Z. Zeng, S. Bao, M. Wang, X. Qi, Z. Fan, H. Zhang, *Nat. Commun.* **2013**, *4*, 1444.
[39] K. Gelderman, L. Lee, S. W. Donne, *J. Chem. Educ.* **2007**, *84*, 685.
[40] J. Hong, X. Xia, Y. Wang, R. Xu, *J. Mater. Chem.* **2012**, *22*, 15006.
[41] H. J. Li, B. W. Sun, L. Sui, D. J. Qian, M. Chen, *Phys. Chem. Chem. Phys.* **2015**, *17*, 3309.
[42] C. Liu, F. Qiu, J. J. Peterson, T. D. Krauss, *J. Phys. Chem. B* **2015**, *119*, 7349.
[43] J. C. Deutsch, *J. Chromatogr. A* **2000**, *881*, 299.
[44] K. Han, M. Wang, S. Zhang, S. Wu, Y. Yang, L. Sun, *Chem. Commun.* **2015**, *51*, 7008.
[45] Z. Ning, O. Voznyy, J. Pan, S. Hoogland, V. Adinolfi, J. Xu, M. Li, A. R. Kirmani, J.-P. Sun, J. Minor, K. W. Kemp, H. Dong, L. Rollny, A. Labelle, G. Carey, B. Sutherland, I. Hill, A. Amassian, H. Liu, J. Tang, O. M. Bakr, E. H. Sargent, *Nat. Mater.* **2014**, *13*, 822.
[46] R. Wang, Y. Shang, P. Kanjanaboos, W. Zhou, Z. Ning, E. H. Sargent, *Energy Environ. Sci.* **2016**, *9*, 1130.